Design, Dynamic Simulation, and Prototyping of a Dual-Axis Solar Tracker Using a Slider-Crank Mechanism

Ahmed Saber
College of Engineering and Technology, American University of the Middle East, Kuwait
ahmed.saber@aum.edu.kw

Mohammad Al Sharah
College of Engineering and Technology, American University of the Middle East, Kuwait
66612@aum.edu.kw

Yahya Al Tamimi
College of Engineering and Technology, American University of the Middle East, Kuwait
60069@aum.edu.kw

Semaan Amine
College of Engineering and Technology, American University of the Middle East, Kuwait
semaan.amine@aum.edu.kw

Eddie Gazo Hanna
College of Engineering and Technology, American University of the Middle East, Kuwait
eddie-hanna@aum.edu.kw (corresponding author)

Received: 30 May 2025 | Revised: 19 June 2025 | Accepted: 28 June 2025

 DOI: https://doi.org/10.48084/etasr.12414

ABSTRACT

Solar trackers improve the photovoltaic energy output by keeping panels aligned with the sun throughout the day. This study introduces a novel, dual-axis solar tracking system driven by an inverted slider-crank mechanism. This system is designed to reduce the mechanical complexity and improve the energy efficiency compared to conventional tracking systems. The kinematic behavior was analyzed using GIM software and the torque and load requirements were evaluated utilizing dynamic simulation in SolidWorks Motion. Finite Element Analysis (FEA) was deployed to assess the structural integrity under wind loads. The system provided a reliable tracking accuracy, smooth motion, and acceptable stress levels with a practical Factor of Safety (FOS). A prototype was built to confirm the effectiveness of the mechanism, offering a compact, low-maintenance alternative to traditional dual-axis trackers, supporting the use of solar technologies in regions with high irradiance.

Keywords-dual-axis solar tracker; slider-crank mechanism; renewable energy; kinematics; stress analysis

I. INTRODUCTION

Solar energy is an efficient solution for the growing energy demands, reducing the environmental impact of fossil fuel usage. Despite the significant advances in Photovoltaic (PV) technology, the ability to convert the solar energy is still highly dependent on the orientation of PV panels. Fixed and single-axis tracking systems are simpler but fail to fully capture the solar radiation throughout the day and across seasons. Dual-axis solar trackers, on the other hand, adjust both the azimuth and elevation angles, allowing them to maintain an optimal angle of reflection, increasing the energy output by up to 45% compared to stationary systems [1-3]. The urgent need for sustainable energy solutions has increased the development of renewable energy technologies, particularly solar power [4-8]. Countries in the Gulf region, such as Saudi Arabia, the United Arab Emirates, Kuwait, Oman, Bahrain, and Qatar, have the highest average solar radiation levels globally (6.0-6.3 kWh/m²/day), making them ideal locations for large-scale solar

power installations [9-11]. Experimental studies have shown that the mobile tracking systems significantly outperform the fixed panels. Comparative analyses reveal that adding one or two Degrees of Freedom (1-DoF or 2-DoF) can increase the energy yields by 25% to over 40% [12-16]. Although various designs use worm screws, linear actuators, and chain transmissions, most of them focus primarily on electronic control and sun-position detection algorithms, neglecting the mechanical efficiency and actuator energy consumption [17, 18]. The inverted slider-crank mechanism is a simpler and more energy-efficient alternative to these methods for dual-axis actuation. Solar tracking systems use intelligent control systems and real-time environmental adjustments to improve the tracking precision and robustness [19-22]. Dual-axis trackers still face mechanical challenges, including complexity, high maintenance requirements, and vulnerability to stresses, such as wind loads [23]. For large-scale solar installations, achieving mechanical stability and load management is critical, so the usage of parallel actuators or reinforced structures is important [24-26]. This study presents a novel dual-axis solar tracking system based on an inverted slider-crank mechanism, as shown in Figure 1. The design is simple, reliable, and energy efficient. Kinematic and dynamic analyses were conducted using GIM [27-29] and SolidWorks software to evaluate the motion profiles and actuation force requirements. Additionally, a static structural analysis was performed under simulated wind loading to ensure the mechanical integrity and identify the potential failure points. Furthermore, this study aims to maximize the PV energy conversion efficiency through precise sun tracking. Its purpose is also to promote the adoption of dual-axis trackers and advance the transition toward sustainable, high-efficiency energy systems.

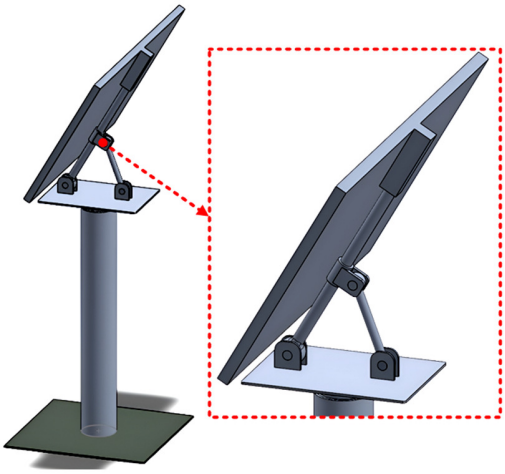

Fig. 1. Geometric model of the solar tracking mechanism designed in SOLIDWORKS.

II. KINEMATIC ANALYSIS

The kinematic analysis was conducted under the assumption of constant crank rotation (N_2=2 rpm, α_2=0 rad/s²). The *X-Y* coordinate system was established, with the origin positioned at point O_2, as depicted in Figure 2, and all angles were measured counterclockwise from the horizontal *X*-axis. The following definition was proposed: link 1 (ground) has length c and angle θ_1, link 2 (crank) has length a and angle θ_2 and link 3 has length L_3, horizontal displacement b, and angle θ_3. Link 4 is a prismatic joint that functions as a slider. In this study, the dimensional synthesis [30-32] was performed using the GIM software to determine the appropriate dimensions, as presented in Table I, of the proposed mechanism necessary to accomplish the desired motion.

TABLE I. OPTIMIZED DIMENSIONS OF THE PROPOSED MECHANISM

Crank length a	**366 mm**
Ground length c	400 mm
Connecting rod length L_3	1100 mm
Crank angle θ_2	[20°, 120°]

The vector loop method is used to analyze the mechanism's kinematics, which was applied to different types of linkages, including four-bar and slider-crank mechanisms [33]. The model is simplified through the use of position vectors to represent each link, thereby forming a closed loop, as illustrated in Figure 2. This approach enables the application of vector equations, facilitating the solution for unknown positions, velocities, and accelerations.

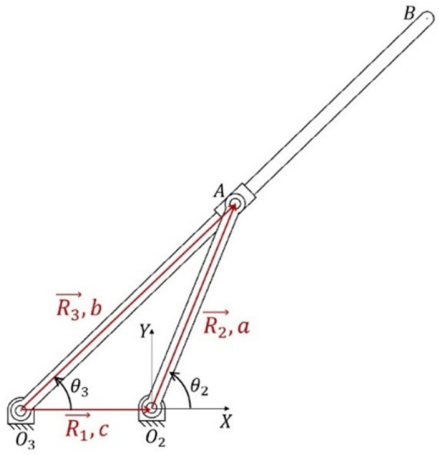

Fig. 2. Vector loops of the mechanism considered for synthesis.

A. Position Analysis

The position vector loop for the slider-crank mechanism O_2AO_3 is:

$$\overrightarrow{R_2} - \overrightarrow{R_3} + \overrightarrow{R_1} = \vec{0} \quad (1)$$

Parameters *a*, *b,* and *c* are the scalar lengths:

$$ae^{j\theta_2} - be^{j\theta_3} + ce^{j\theta_1} = 0 \quad (2)$$

This results in two scalar equations that can be solved simultaneously for θ_3 and the position of the slider b:

$$\theta_3 = \tan^{-1}\left(\frac{a\sin\theta_2}{a\cos\theta_2 + c}\right) \quad (3)$$

$$b = \sqrt{a^2 + c^2 + 2ac\cos\theta_2} \quad (4)$$

B. Velocity Analysis

To find the angular velocity of link 3 and the linear velocity of the slider, (2) was differentiated with respect to time:

$$ja\omega_2 e^{j\theta_2} - jb\omega_3 e^{j\theta_3} = 0 \quad (5)$$

from which, two scalar equations can be solved simultaneously for ω_3 and the velocity of the slider $\dot{b}$:

$$\omega_3 = \frac{a\omega_2}{b}\cos(\theta_2 - \theta_3) \quad (6)$$

$$\dot{b} = \sqrt{a^2\omega_2^2 + b^2\omega_3^2 - 2ab\omega_2\omega_3\cos(\theta_2 - \theta_3)} \quad (7)$$

To find the angular acceleration of link 3 and the linear acceleration of the slider, (5) will be differentiated with respect to time:

$$\left(a\alpha_2 je^{j\theta_2} - a\omega_2^2 e^{j\theta_2}\right) - \left(b\alpha_3 je^{j\theta_3} - b\omega_3^2 e^{j\theta_3}\right) = 0 \quad (8)$$

This leads to two scalar equations that can be solved simultaneously for α_3 and $\ddot{b}$:

$$\begin{bmatrix} -\cos\theta_3 & b\sin\theta_3 \\ -\sin\theta_3 & -b\cos\theta_3 \end{bmatrix}\begin{bmatrix} \ddot{b} \\ \alpha_3 \end{bmatrix} = \begin{bmatrix} B \\ A \end{bmatrix} \quad (9)$$

where:

$$A = -a\alpha_2\cos\theta_2 + a\omega_2^2\sin\theta_2 + 2\dot{b}\omega_3\cos\theta_3 - b\omega_3^2\sin\theta_3 \quad (10)$$

and

$$B = a\alpha_2\sin\theta_2 a\omega_2^2\cos\theta_2 - 2\dot{b}\omega_3\sin\theta_3 - b\omega_3^2\cos\theta_3 \quad (11)$$

The acceleration analysis of the slider link 4 gives:

$$a_{Ax} = -a\cos\theta_2\,(\alpha_2 + \omega_2^2) \quad (12)$$

$$a_{Ay} = a\sin\theta_2\,(\alpha_2 - \omega_2^2) \quad (13)$$

III. DYNAMIC FORCE ANALYSIS

To determine the internal forces and torque in the system, dynamic force analysis is performed using Newton's laws as:

$$\sum \vec{F} = m\overrightarrow{a_G} \quad (14)$$

$$\sum \vec{T} = I_G\alpha \quad (15)$$

These equations are projected in the rectangular coordinate system, leading to:

$$\sum F_x = ma_{Gx} \quad \sum F_y = ma_{Gy} \quad \sum T = I_G\alpha \quad (16)$$

where m is the mass, a_{Gx} and a_{Gy} are the linear accelerations of the center of mass, I_G is the mass moment of inertia calculated at the center of mass, and α is the angular acceleration. These equations are applicable to each moving body in the system, as portrayed in Figure 3.

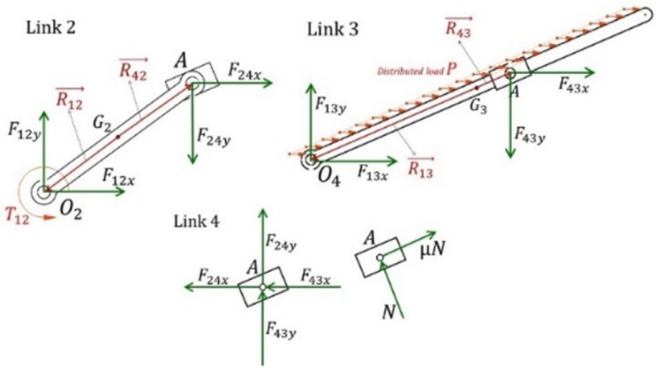

Fig. 3. Free body diagrams of each link.

This results in a set of linear simultaneous equations, which are solved using a matrix method. The only force that exists at the interface between link 4 and 3 is friction. Assuming Coulomb friction, the x and y components of the force at this interface can be expressed as:

$$F_{43x} = N(\sin\theta_3 \pm \mu\cos\theta_3) \quad (17)$$

$$F_{43y} = -N(\cos\theta_3 \pm \mu\sin\theta_3) \quad (18)$$

Link 3 is also subjected to a distributed load P, which represents the wind force. A set of eight equations has been formulated to ascertain eight parameters: the forces F_{12x}, $F_{12y}, F_{13x}, F_{13y}, F_{24x}, F_{24y}, N,$ and the input torque T_{12}. The dimensions of the link lengths and positions, the locations of the links' Centers of Gravity (CGs), the linear accelerations of those CGs, and the angular accelerations and velocities of the links have all been previously determined through kinematic analysis. Subsequently, these equations can be used to assemble the matrices and ascertain the solutions:

$$\begin{bmatrix} 1 & 0 & 1 & 0 & 0 & 0 & 0 & 0 \\ 0 & 1 & 0 & 1 & 0 & 0 & 0 & 0 \\ -R_{12y} & R_{12x} & 0 & 0 & -R_{42y} & R_{42x} & 0 & 1 \\ 0 & 0 & 1 & 0 & 0 & 0 & \sin\theta_3 - \mu\cos\theta_3 & 0 \\ 0 & 0 & 0 & 1 & 0 & 0 & \cos\theta_3 + \mu\sin\theta_3 & 0 \\ 0 & 0 & -R_{13y} & R_{13x} & 0 & 0 & R_{43x}(\cos\theta_3 + \mu\sin\theta_3) - R_{43y}(\sin\theta_3 - \mu\cos\theta_3) & 0 \\ 0 & 0 & 0 & 0 & 1 & 0 & \sin\theta_3 - \mu\cos\theta_3 & 0 \\ 0 & 0 & 0 & 0 & 0 & 1 & -\cos\theta_3 - \mu\sin\theta_3 & 0 \end{bmatrix} \times \begin{bmatrix} F_{12x} \\ F_{12y} \\ F_{13x} \\ F_{13y} \\ F_{24x} \\ F_{24y} \\ N \\ T_{12} \end{bmatrix} = \begin{bmatrix} m_2a_{G2x} \\ m_2a_{G2x} \\ I_{G2}\alpha_2 \\ m_3a_{G3x} - PL_3 \\ m_3a_{G3y} \\ I_{G3}\alpha_3 \\ m_4a_{Ax} \\ m_4a_{Ay} \end{bmatrix} \quad (19)$$

IV. STATIC ANALYSIS

Static stress analysis was performed to determine the structural performance of the solar tracking mechanism under expected operational loads. The objective of this analysis is threefold: first, to identify the critical stress regions; second, to evaluate the deformation behavior; and third, to ensure that the design meets the safety and reliability requirements. The mechanism was modeled in SOLIDWORKS, and the simulation was executed using its integrated FEA tools to assess the stress distribution, displacement, and FOS. The structural components, including the supporting beams, were fabricated from aluminum 1060 alloy, which was selected for its high strength-to-weight ratio and corrosion resistance and

the material properties are presented in Table II. In order to simulate realistic loading conditions, the solar tracking mechanism is constrained by fixing the lower plate. Two loads were applied to the solar panel surface: a vertical load to represent the panel's self-weight, and a horizontal load to simulate the effect of wind, as shown in Figure 4(a). The analysis was conducted at an inclination angle of 60° (θ_3), which represents a typical operating position of the solar panel. The panel is assigned a mass of 21 kg [34], resulting in a gravitational force of 206.01 N.

TABLE II. MECHANICAL PROPERTIES OF ALUMINUM 6061 ALLOY

Elastic modulus	**69,000 MPa**
Poisson's ratio	0.33
Shear modulus	27,000 MPa
Mass density	2,700 Kg/m^3
Tensile strength	68.9356 MPa
Yield strength	27.5742 MPa

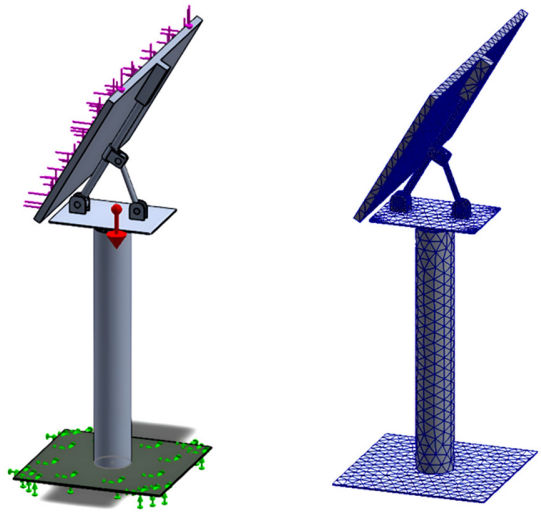

(a) (b)

Fig. 4. Loads and boundary conditions: (a) fixtures (green), loads (purple), gravity (red); (b) generated mesh structure.

The wind load is estimated using the standard drag force equation [35]:

$$P = \frac{1}{2}\rho V^2 A C_D \quad (20)$$

where P is the wind force, ρ is the air density (1.225 kg/m³), V is the wind velocity set at 4.5 m/s based on the meteorological data for Kuwait [36], A is the projected area of the panel (1.0 m × 1.7 m), and C_D is the drag coefficient. The drag coefficient is calculated using the empirical formula [35]:

$$C_D = 1.1 + 0.02\left(\frac{L_3}{D} + \frac{D}{L_3}\right) \quad (21)$$

where L_3 and D are the length and depth of the panel, respectively. The resultant wind force is calculated to be 24.158 N, and it is observed that all contacts between the components of the mechanism are classified as bonded, under the assumption that no relative motion or separation will occur under the load. The finite element mesh is automatically generated using the default fine mesh setting in SOLIDWORKS, resulting in a total of 12,774 elements, as displayed in Figure 4(b).

V. TORQUE ANALYSIS

To ensure a reliable and safe operation, it is important to determine the driving torque of an appropriately sized motor. In this study, SOLIDWORKS motion analysis was used to estimate the required driving torque for the proposed solar tracker system. The design presents an inverted slider-crank mechanism driven by a motor mounted at the hinge O_2. The motor operates at a constant speed of 2 rpm, initiating from an initial crank angle of θ_2 = 20°. The simulation lasts eight sec during which the crank executes the specified motion.

VI. RESULTS AND DISCUSSION

The outcomes of the kinematic, dynamic, and static analyses conducted on the proposed dual-axis solar tracking system, are presented as well as the validation through prototype testing. The motion behavior of the inverted slider-crank mechanism was initially determined through the usage of analytical models developed in MATLAB and simulations generated by the GIM software, as illustrated in Figure 5.

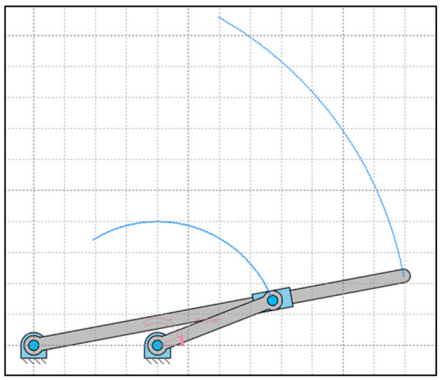

Fig. 5. Simulation of the optimized inverted slider-crank mechanism operation.

The relationship between the crank input angle (θ_2) and the resulting tilt angle of the solar panel (θ_3) was determined and the findings yielded a high degree of agreement between the analytical and simulated values, as shown in Figure 6, thus validating the kinematic model. The smooth variation of θ_3 with respect to θ_2 indicates a stable motion and effective sun tracking capability. Additionally, an analysis of the kinematic behavior of point A was conducted, corresponding to the slider-crank joint that controls the solar panel's motion. The analysis was performed to calculate the inertial forces acting on the system. As presented in Figures 7 and 8, the acceleration components of point A are examined in the horizontal (X) and vertical (Y) directions, respectively, as a function of the crank input angle (θ_2). The acceleration values were calculated using both MATLAB and GIM software, and the results demonstrated an excellent agreement between the two methods. This finding validates the accuracy of the dynamic model and the horizontal acceleration a_{Ax} displays a seamless transition from negative to positive values, thereby reflecting

the slider's directional change during movement. In contrast, the vertical acceleration a_{Ay} follows a parabolic trajectory, indicating a decelerating downward motion followed by an upward acceleration. The precise estimation of these acceleration components is important for calculating the dynamic forces and, consequently, the motor torque required to drive the mechanism. This analysis guarantees that the actuator selection is based on realistic dynamic loading conditions, enhancing the reliability and efficiency of the solar tracking system.

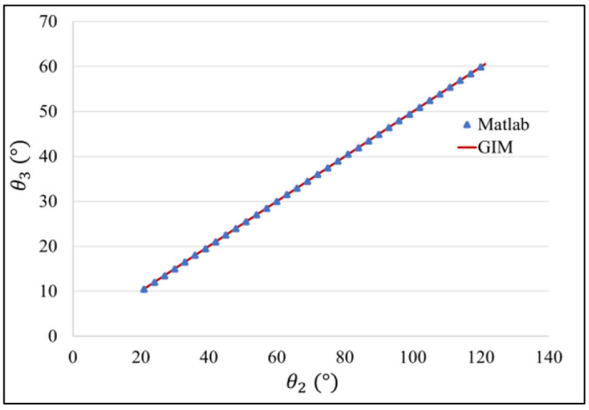

Fig. 6. Solar panel angle (θ_3) versus crank rotation (θ_2).

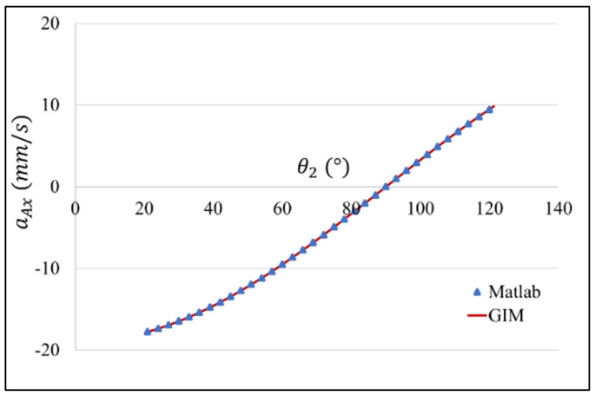

Fig. 7. Acceleration of point A for the optimized design in direction *X*.

The validated kinematics were then used to conduct a dynamic force analysis, according to the Newton-Euler equations. The resulting inertial forces and input torques were subsequently utilized to appropriately size the actuation system. The torque simulations conducted in SOLIDWORKS motion indicated that the system requires a driving torque ranging between 120 N·m and 250 N·m during a complete drive cycle, as exhibited in Figure 9. The simulation analyzed both the gravitational and wind loads, modeled under typical conditions for Kuwait. The results of the study indicated a maximum von Mises stress of 9.67 MPa and a peak deformation of 2.74 mm, as shown in Figures 10 (a) and 10 (b). The calculated FOS across the structure exceeded 2.85, as presented in Figure 10 (c), indicating that the design is structurally sound under the expected loading scenarios. These outcomes substantiate the selection of materials and geometry for the mechanism's components. This type of information is critical for selecting a motor with sufficient torque while optimizing the energy efficiency.

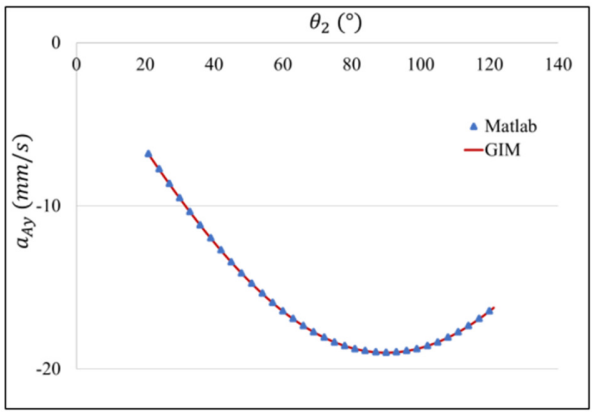

Fig. 8. Acceleration of point A for the optimized design in direction *Y*.

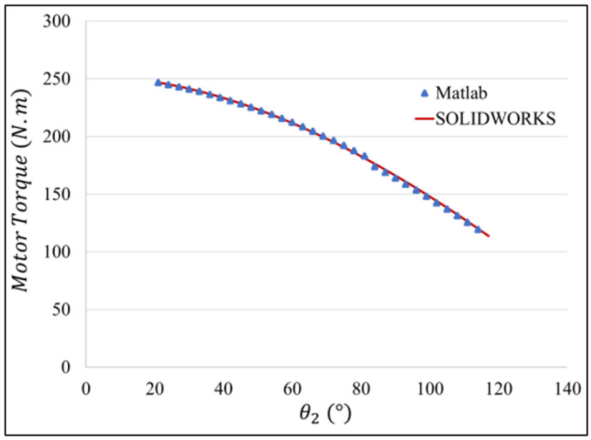

Fig. 9. Driving torque of the slider-crank mechanism.

VII. PROTOTYPE

To validate the proposed design, a functional prototype of the dual-axis solar tracking system was developed, as illustrated in Figure 11. The structure is constructed with a lightweight aluminum frame mounted on a steel base plate, which provides support for a 50 W polycrystalline solar panel. The tracking motion is achieved using two MG996R servo motors. The operation of these motors is directed by an Arduino Uno microcontroller, which processes the input from four LDRs arranged in a quadrant configuration. This configuration is used to ascertain the sun's position. Initially, the LDRs were installed behind the panel; however, this resulted in inconsistent tracking due to indirect light exposure. The repositioning of the sensors to the panel frame resulted in a substantial enhancement in the system accuracy and responsiveness, facilitating a more precise alignment with the sun. The control logic is based on a simple voltage comparison between opposing sensors, directing the motors toward the brighter side. The system is powered by a 12-V rechargeable lithium-ion battery, with the control unit located at the base. The wiring is routed internally through the central support column to prevent tangling or movement interference.

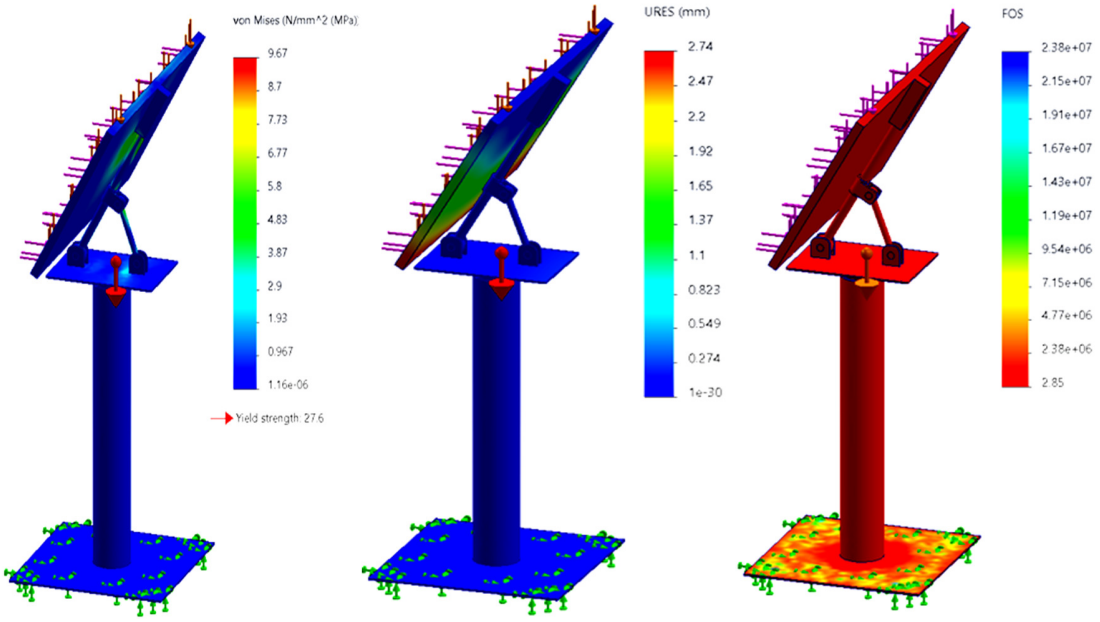

(a) (b) (c)

Fig. 10. Static structural analysis results: (a) stress distribution, (b) deformation, (c) FOS.

The preliminary testing confirmed the mechanism's smooth and reliable operation under typical daylight conditions. The structure remained stable during movement, and the motors responded effectively to the changes in sunlight direction.

Fig. 11. Prototype of the dual-axis solar tracking system showing the aluminum frame structure, mounted solar panel, and servo motor setup for azimuth and elevation control using an Arduino microcontroller.

VIII. CONCLUSIONS

This study presented the design, analysis, and prototyping of a novel dual-axis solar tracking system driven by an inverted slider-crank mechanism. The development of kinematic and dynamic models was facilitated by the GIM software, while the validation of structural integrity was achieved through Finite Element Analysis (FEA) in SOLIDWORKS. The mechanism exhibits consistent tracking performance while maintaining a low level of complexity. The stress analysis confirms an adequate Factor of Safety (FOS) and torque requirements remain within practical limits for the actuator selection. The development of a physical prototype validates the system's feasibility for real-world applications. In summary, the mechanically optimized design offers a cost-effective and energy-efficient solution that enables the advancement of dual-axis solar tracking technologies in renewable energy applications. Subsequent studies will concentrate on integrating an automated control system, conducting long-term field testing, and optimizing the design for enhanced performance and durability.

ACKNOWLEDGMENT

The authors wish to acknowledge Erik Macho, Alfonso Hernández, CompMech, Department of Mechanical Engineering, UPV/EHU, for the permission to use the GIM® software.

REFERENCES

[1] H. Mousazadeh, A. Keyhani, A. Javadi, H. Mobli, K. Abrinia, and A. Sharifi, "A review of principle and sun-tracking methods for maximizing solar systems output," *Renewable and Sustainable Energy Reviews*, vol. 13, no. 8, pp. 1800–1818, Oct. 2009, https://doi.org/10.1016/j.rser.2009.01.022.

[2] Y. Dhuri, S. K. Verma, P. K. Yadav, T. Rizvi, and D. Bhonsle, "Improvement in Efficacy of Solar System using Dual Axis Solar Tracking System," *International Journal of Innovative Research in Engineering*, vol. 3, no. 2, pp. 110–113, Apr. 2022.

[3] M. Haneef *et al.*, "Optimization of a novel lead-free MASiI3 based perovskite solar cell: A comprehensive study on device performance enhancement," *Results in Engineering*, vol. 23, p. 102809, Sep. 2024, https://doi.org/10.1016/j.rineng.2024.102809.

[4] K. Solaun and E. Cerdá, "Climate change impacts on renewable energy generation. A review of quantitative projections," *Renewable and Sustainable Energy Reviews*, vol. 116, Dec. 2019, Art. no. 109415, https://doi.org/10.1016/j.rser.2019.109415.

[5] A. I. Osman, N. Mehta, and A. M. Elgarahy, "Renewable energy technologies for sustainable future: A comprehensive review," *Energy Conversion and Management*, vol. 274, 2023, Art. no. 116377.

[6] H. Hijazi, O. Mokhiamar, and O. Elsamni, "Mechanical design of a low cost parabolic solar dish concentrator," *Alexandria Engineering Journal*, vol. 55, no. 1, pp. 1–11, Mar. 2016, https://doi.org/10.1016/j.aej.2016.01.028.

[7] M. A. Alazwari *et al.*, "Assessment of photovoltaic system in existence of nanomaterial cooling flow," *Results in Engineering*, vol. 24, Dec. 2024, Art. no. 103264, https://doi.org/10.1016/j.rineng.2024.103264.

[8] M. E. Bendib and A. Mekias, "Solar Panel and Wireless Power Transmission System as a Smart Grid for Electric Vehicles," *Engineering, Technology & Applied Science Research*, vol. 10, no. 3, pp. 5683–5688, Jun. 2020, https://doi.org/10.48084/etasr.3473.

[9] H. Z. Al Garni and A. Awasthi, "Solar PV power plant site selection using a GIS-AHP based approach with application in Saudi Arabia," *Applied Energy*, vol. 206, pp. 1225–1240, Nov. 2017, https://doi.org/10.1016/j.apenergy.2017.10.024.

[10] W. Ahmed, J. A. Sheikh, and M. A. P. Mahmud, "Impact of PV System Tracking on Energy Production and Climate Change," *Energies*, vol. 14, no. 17, Jan. 2021, Art. no. 5348, https://doi.org/10.3390/en14175348.

[11] S. Grami and Y. Gharbia, "Experimental investigation of new designed solar parabolic trough collectors," in *2018 IEEE International Conference on Industrial Technology (ICIT)*, Lyon, France, Oct. 2018, pp. 972–977, https://doi.org/10.1109/ICIT.2018.8352310.

[12] A. Karabiber and Y. Güneş, "Single-Motor and Dual-Axis Solar Tracking System for Micro Photovoltaic Power Plants," *Journal of Solar Energy Engineering*, vol. 145, no. 051004, Feb. 2023, https://doi.org/10.1115/1.4056739.

[13] M. J. Ya'u, "A Review on Solar Tracking Systems and Their Classifications," *Journal of Energy, Environmental & Chemical Engineering*, vol. 2, no. 3, pp. 46–50, Aug. 2017, https://doi.org/10.11648/j.jeece.20170203.12.

[14] E. A. Shokralla *et al.*, "Improvement of structural, morphological and thermoelectric power factor of thermally evaporated Sr doped SnTe film," *Ceramics International*, vol. 50, no. 18, Part B, pp. 34467–34471, Sep. 2024, https://doi.org/10.1016/j.ceramint.2024.06.200.

[15] H. A. Kazem, M. T. Chaichan, A. H. A. H. Al-Waeli, and K. Sopian, "Dual axis solar photovoltaic trackers: An in-depth review," *Energy Sources, Part A: Recovery, Utilization, and Environmental Effects*, vol. 46, no. 1, pp. 15331–15356, Dec. 2024, https://doi.org/10.1080/15567036.2024.2420781.

[16] A. Awasthi *et al.*, "Review on sun tracking technology in solar PV system," *Energy Reports*, vol. 6, pp. 392–405, Nov. 2020, https://doi.org/10.1016/j.egyr.2020.02.004.

[17] M. Efendi, R. I. Mainil, and A. Aziz, "Comparison of the Efficiency of Solar PV Fixed, Single-Axis, and Dual-Axis Solar Trackers: A Review," *Jurnal Konversi Energi dan Manufaktur*, pp. 84–93, Jan. 2025, https://doi.org/10.21009/JKEM.10.1.9.

[18] H. M. Fahad, A. Islam, M. Islam, Md. F. Hasan, W. F. Brishty, and Md. M. Rahman, "Comparative Analysis of Dual and Single Axis Solar Tracking System Considering Cloud Cover," in *2019 International Conference on Energy and Power Engineering (ICEPE)*, Dhaka, Bangladesh, Mar. 2019, pp. 1–5, https://doi.org/10.1109/CEPE.2019.8726646.

[19] N. Thungsuk *et al.*, "Performance Analysis of Solar Tracking Systems by Five-Position Angles with a Single Axis and Dual Axis," *Energies*, vol. 16, no. 16, Jan. 2023, Art. no. 5869, https://doi.org/10.3390/en16165869.

[20] S. Amine and O. Mokhiamar, "A study of stability and power consumption of electric vehicles using different modern control strategies," *Alexandria Engineering Journal*, vol. 58, no. 4, pp. 1281–1290, Dec. 2019, https://doi.org/10.1016/j.aej.2019.10.010.

[21] M. H. Chamas, S. Amine, E. Gazo Hanna, and O. Mokhiamar, "Control of a Novel Parallel Mechanism for the Stabilization of Unmanned Aerial Vehicles," *Applied Sciences*, vol. 13, no. 15, Jan. 2023, Art. no. 8740, https://doi.org/10.3390/app13158740.

[22] U. Mamodiya, I. Kishor, M. A. Almaiah, M. Hamdi, R. Shehab, and T. Alkhdour, "Numerical modeling and neural network optimization for advanced solar panel efficiency," *Scientific Reports*, vol. 15, no. 1, Jul. 2025, Art. no. 23492, https://doi.org/10.1038/s41598-025-06830-z.

[23] R. Rotar, F. M. Petcuț, R. Susany, F. Oprițoiu, and M. Vlăduțiu, "Dependability Assessment of a Dual-Axis Solar Tracking Prototype Using a Maintenance-Oriented Metric System," *Applied System Innovation*, vol. 7, no. 4, Aug. 2024, Art. no. 67, https://doi.org/10.3390/asi7040067.

[24] O. Altuzarra, E. Macho, J. Aginaga, and V. Petuya, "Design of a solar tracking parallel mechanism with low energy consumption," *Proceedings of the Institution of Mechanical Engineers, Part C: Journal of Mechanical Engineering Science*, vol. 229, no. 3, pp. 566–579, Feb. 2015, https://doi.org/10.1177/0954406214537249.

[25] S. Grami and Y. Gharbia, "GMS friction compensation in robot manipulator," in *IECON 2013 - 39th Annual Conference of the IEEE Industrial Electronics Society*, Vienna, Austria, Aug. 2013, pp. 3555–3560, https://doi.org/10.1109/IECON.2013.6699700.

[26] E. Daisy, "Structural Integrity and Performance Evaluation of Solar Tracker Components Using Finite Element Simulation and Material Selection Criteria," Aug. 2024.

[27] E. Macho, M. Urízar, V. Petuya, and A. Hernández, "Improving Skills in Mechanism and Machine Science Using GIM Software," *Applied Sciences*, vol. 11, no. 17, Jan. 2021, Art. no. 7850, https://doi.org/10.3390/app11177850.

[28] V. Petuya, E. Macho, O. Altuzarra, C. Pinto, and A. Hernandez, "Educational software tools for the kinematic analysis of mechanisms," *Computer Applications in Engineering Education*, vol. 22, no. 1, pp. 72–86, 2014, https://doi.org/10.1002/cae.20532.

[29] M. AlJaimaz, H. AlDousari, F. Ebrahem, D. AlZayyan, E. G. Hanna, and Z. AlMazidi, "Kinematic Analysis of a Variable Speed Deep Drawing Press Using GIM Software," in *World Congress on Mechanical, Chemical, and Material Engineering*, London, UK, Aug. 2023, https://doi.org/10.11159/icmie23.142.

[30] M. S. Jo, J. K. Shim, H. S. Park, and W. R. Kim, "Dimensional Synthesis of Watt II and Stephenson III Six-Bar Slider-Crank Function Generators for Nine Prescribed Positions," *Applied Sciences*, vol. 12, no. 20, Jan. 2022, Art. no. 10503, https://doi.org/10.3390/app122010503.

[31] E. Gazo-Hanna, A. Saber, and S. Amine, "Design and Modeling of a Six-Bar Mechanism for Repetitive Tasks with Symmetrical End-Effector Motion," *Engineering, Technology & Applied Science Research*, vol. 14, no. 5, pp. 16302–16310, Oct. 2024, https://doi.org/10.48084/etasr.8139.

[32] S. Amine, B. Prasad, A. Saber, O. Mokhiamar, and E. Gazo-Hanna, "Design and Analysis of a Planar Six-Bar Crank-Driven Leg Mechanism for Walking Robots," *Applied Sciences*, vol. 14, no. 19, Jan. 2024, Art. no. 8919, https://doi.org/10.3390/app14198919.

[33] R. L. Norton, *Design of Machinery: An Introduction to the Synthesis and Analysis of Mechanisms and Machines*, 3rd ed. Boston, MA, USA: Mcgraw-Hill College, 2004.

[34] "Solar Panel Sizes & Dimensions – Complete Guide for 2025," *JLM Energy*, May 09, 2025. https://www.jlmenergy.co.uk/blog/solar-panel-sizes-dimensions-guide/.

[35] Y. Cengel and J. Cimbala, *Fluid Mechanics Fundamentals and Applications*, 3rd ed. New York, NY, USA: McGraw Hill, 2014.

[36] M. Adouane, A. Al-Qattan, B. Alabdulrazzaq, and A. Fakhraldeen, "Comparative performance evaluation of different photovoltaic modules technologies under Kuwait harsh climatic conditions," *Energy Reports*, vol. 6, pp. 2689–2696, Nov. 2020, https://doi.org/10.1016/j.egyr.2020.09.034.